Charged Polymeric Brushes: Structure and Scaling Relations

R. Israëls,*,† F. A. M. Leermakers, and G. J. Fleer

Department of Physical and Colloid Chemistry, Wageningen Agricultural University, Dreijenplein 6, 6703 HB Wageningen, The Netherlands

E. B. Zhulina

Institute of Macromolecular Compounds of the Russian Academy of Sciences, 199004 St. Petersburg, Russia

Received October 12, 1993; Revised Manuscript Received March 21, 1994®

ABSTRACT: We present numerical results from a self-consistent (mean)-field (SCF) model for the structure and scaling behavior of charged brushes and compare these with predictions of an analytical SCF model on the same system. The parameters we consider in this study are the chain length N, the average surface area σ per anchored chain, the average distance m between neighboring charges on the chains, and the salt concentration ϕ_s. At high anchoring densities, three different regimes of brush behavior may be distinguished. In the salt-free case, the behavior of the brush is dominated either by electrostatic interactions at high charge densities (*osmotic brush*) or by nonelectrostatic excluded-volume interactions at low charge densities (*quasi-neutral brush*). Upon adding salt in the solution, a third regime can be found (*salted brush*). The behavior in this regime, although resulting from electrostatic interactions, is very similar to that in a neutral brush and can effectively be described using an electrostatic excluded-volume parameter $v_{el} \sim \phi_s^{-1} m^{-2}$. We find excellent agreement regarding structure as well as scaling relations between the two theories in these three (high anchoring density) regimes. At extremely low anchoring densities, agreement between the two theories is less good. This is due to the breakdown at low densities of the mean-field approximation presently used in the numerical model. In between, at intermediate anchoring density the analytical theory predicts a very peculiar regime, where the thickness H scales as $H \sim N^3 \sigma^{-1} m^{-2}$. This so-called "*Pincus brush*", named after the author who originally described it, is not recovered with the numerical theory. For the wide range of parameters used, we find the *Pincus regime* is too small to be detected. This is probably true for any reasonable set of parameters.

I. Introduction

During the last decade, a considerable amount of effort has been spent on the theoretical analysis of polymer brushes, i.e., layers of polymer chains fixed by one end at impermeable surfaces of various geometries. Typical examples of such systems are the supermolecular structures that are formed in melts and solutions of block copolymers with incompatible blocks. Brushlike structures are also present in the adsorption layers formed by block copolymers with selectively adsorbing blocks. The practical relevance of these systems is that the brush forms a stabilizing coating on colloid particles, preventing aggregation.

The behavior of neutral polymer brushes under various conditions is rather well understood. Not only the scaling dependences for the average brush characteristics, but also the fine details of the intrinsic brush structure predicted theoretically are in reasonable agreement with experimental observations (see, e.g., the review by Halperin et al.[1]).

Charged brushes, i.e., brushes formed by polymer chains containing ionizable groups, have been investigated to a lesser extent than neutral ones. This is due to the complexity of the system, which arises from the appearance of long-range electrostatic interactions in a charged brush. Scaling analyses of a planar polyelectrolyte brush[2–4] revealed a much more complex behavior than that of neutral brushes.

Pincus was the first to show that, depending on the degree of charge of the chain and the grafting density, a polyelectrolyte brush can exhibit two different types of behavior:[2] it either can be strongly charged, loosing its mobile counterions (*Pincus regime*), or conserve the counterions mainly inside the brush and, thus, be practically electroneutral (*osmotic regime*). Borisov et al.[5] argued that at high grafting densities the excluded-volume interactions between noncharged units dominate over electrostatic interactions, leading to the *quasi-neutral* regime.

If the salt concentration in solution exceeds by far the concentration of counterions in the brush, the so-called salt-dominance regime (*salted brush*) is found.[2–4] The scaling dependences of the brush thickness in this regime are similar to those in the uncharged brush: the interactions in the brush can be described by an *effective* second virial coefficient incorporating both nonelectrostatic and electrostatic interactions.

Some attempts have been carried out to analyze the intrinsic brush structure, the distribution of counterions and that of the electrostatic field. Based on the solution of the Poisson–Boltzmann equation for the electrostatic field in a brush, segment density profiles were calculated numerically.[7,8] An asymptotical analytical solution for brush characteristics was obtained by Zhulina et al.[3] under the simplifying assumption of local electroneutrality in the brush. It was shown that, contrary to the case of a neutral brush, where the shape of the segment density profile is sensitive to the solvent quality (parabolic under the conditions of athermal solvent, sharpening gradually with decreasing solvent quality[1,9,18,19,20]), the distribution of segments in a polyelectrolyte brush is described by a Gaussian function over a wide range of solvent qualities. Only at solvencies that are worse than that of a Θ-solvent ($\chi > 0.5$), the brush collapses abruptly.

In the present paper we present the analysis of polyelectrolyte brushes, using the self-consistent-field approach developed originally by Scheutjens and Fleer[10,11] to describe the adsorption of uncharged homopolymers. It

† Present address: Department of Materials Science and Engineering, University of Pittsburgh, Pittsburgh, PA 15261.

® Abstract published in *Advance ACS Abstracts*, May 1, 1994.

0024-9297/94/2227-3249$04.50/0

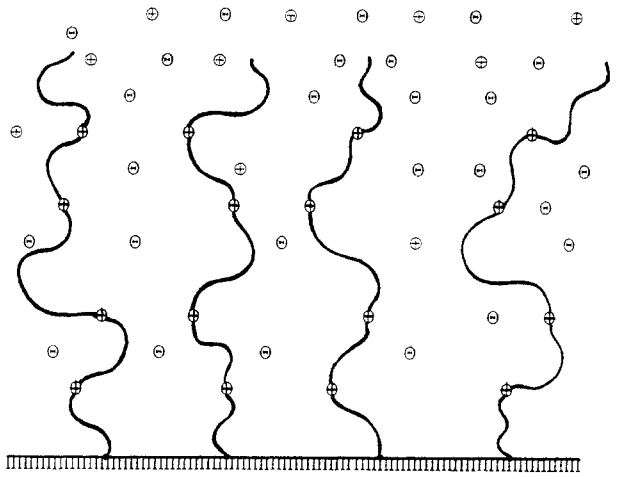

Figure 1. Schematic picture of a charged brush. The positively charged chains are grafted to a flat interface. Co-ions and counterions are free to move inside the brush or in the bulk phase.

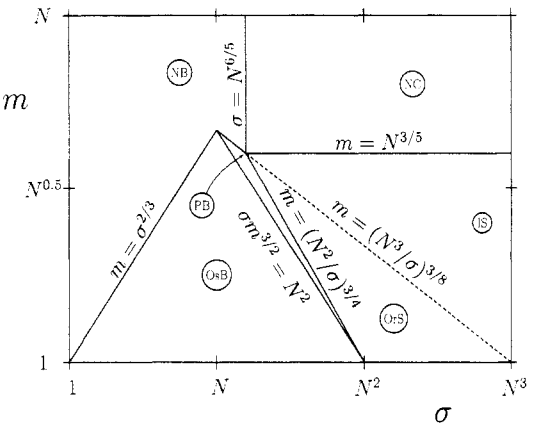

Figure 2. Diagram of states for a charged brush in the absence of external salt. At fixed chain length N, six different regimes may be found, depending on the distance m between charges on the chain and the area σ per grafted molecule: NB (quasi-neutral brush), NC (neutral coils), OsB (osmotic brush), PB (Pincus brush), OrS (oriented sticks), and IS (isotropically distributed sticks). The scaling behavior for the boundaries is given in the figure.

was extended to model brushes by Cosgrove et al.[12] and to electrostatically charged systems by Evers et al.[13,14] With this lattice model, it is possible to obtain a rigorous numerical solution (within the self-consistent mean-field approximation) for the equilibrium characteristics of a polyelectrolyte brush. Thus, a detailed comparison of (asymptotical) analytical predictions with a more exact numerical solution of the brush is possible over a wide range of conditions.

This paper is organized as follows: In section II we present the main results of the analytical theory for a polyelectrolyte brush. Section III outlines the numerical lattice model. Section IV contains the results of comparisons between the two models, and in Section V we summarize the main conclusions.

II. Analytical Model

Definitions. We consider a planar layer formed by long flexible polyelectrolyte chains consisting of N units of size a (with $N \gg 1$). The chains are grafted at one end onto an impermeable surface with an average area per chain denoted by $a^2\sigma$ (Figure 1). Each polymer chain contains $Q = N/m$ ionizable groups, with am being the average distance along the chain between two neighboring charged units. We assume that all polymer chains are positively charged and that each ionizable group carries a charge $+e$. Only weakly charged chains are considered ($m \gg 1$), so that direct electrostatic repulsion along the chain does not lead to electrostatic stiffening.

The grafted layer is in equilibrium with a bulk solution, which contains only solvent (water), and sometimes salt. We take the salt to be symmetrical. Results for asymmetric electrolytes have been published elsewhere.[15] For the present symmetric case, the concentrations of both (monovalent) ions in the bulk are equal and denoted by ϕ_s (expressed as a volume fraction). In theory, one can distinguish chain counterions and salt counterions. In this paper we assume both types of counterions to be identical. Thus, in the grafted layer, we distinguish only the concentration of co-ions (ϕ_+) and the (total) concentration of counterions (ϕ_-).

Below we will introduce four different measures of brush thickness, which we summarize here for quick reference. The thickness H is defined as the upper boundary of the brush, i.e., the distance where the segment density profile drops to zero. A Gaussian profile extends infinitely far: $H = \infty$. Therefore, we define h_0 to be the characteristic length of the (Gaussian) profile for a salt-free brush. H_{rms} is defined as the second moment of a segment density profile. Finally, we will use the rescaled thickness $z = H/h_0$. Note that H, H_{rms}, and h_0 are taken as dimensionless quantities, expressed in units of a.

Scaling-Type Relations. In addition to long-range electrostatic interactions, conventional short-range interactions between noncharged units are also present in the system. The equilibrium structure of a brush is determined by the balance of all intermolecular interactions. Ignoring all numerical coefficients, a rough scaling-type picture of a polyelectrolyte brush has been constructed.[5,6] In Figure 2 we summarize the main results of this treatment. The figure shows a "diagram of states" for a grafted polyelectrolyte brush in (m, σ) coordinates on a logarithmic scale. The brush is assumed to be immersed in a salt-free solution under the conditions of a marginal solvent.

Several different regimes are distinguishable in Figure 2. At high σ (loose grafting), individual coils can behave either as quasi-neutral nonoverlapping chains (NC) at low charge densities (high m) or, if the charge density $1/m$ is high enough, as isotropically distributed sticks (IS). In this IS regime, chains are stretched due to *intra*molecular electrostatic repulsion. *Inter*molecular orientational effects in charged coils appear with decreasing σ, leading to the oriented sticks regime (OrS).

Below the conventional threshold of laterally overlapping chains, three main regimes are possible. Weakly charged ($m \gg 1$) and densely grafted ($\sigma \lesssim N$) brushes exhibit *quasi-neutral* behavior, where nonelectrostatic interactions between units dominate over electrostatic interactions; we call this the quasi-neutral brush (NB). For more highly charged brushes ($m \ll N$), we find either the *osmotic brush* (OsB) or *Pincus brush* (PB) regime. In the osmotic regime, the mobile counterions are located inside the layer and the brush is swollen by the osmotic pressure of the counterions. In the Pincus regime practically all counterions leave the brush and the chains are stretched by the unscreened electrostatic repulsion among units.

The scaling dependences of the brush thickness H in the various regimes are collected in the first five rows of Table 1 (the last two rows will be discussed later). The parameter v in the table is the dimensionless second virial coefficient. The boundaries between any two regimes

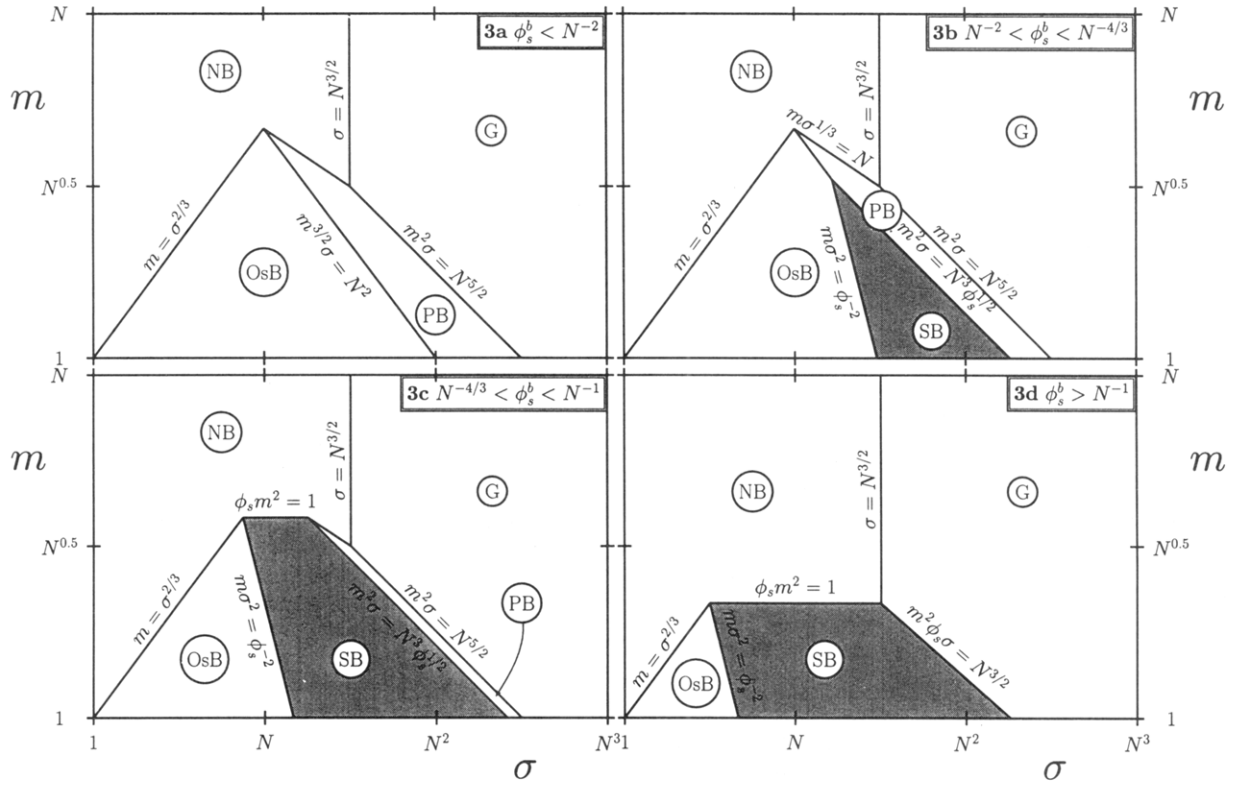

Figure 3. Diagram of states for a charged brush in a mean-field model at fixed N for different salt concentrations $\phi_s < N^{-2}$ (a), $N^{-2} < \phi_s < N^{-4/3}$ (b), $N^{-4/3} < \phi_s < N^{-1}$ (c), and $\phi_s > N^{-1}$ (d). The SB (salted brush) regime is shaded; the expressions for the boundaries are indicated.

Table 1. Scaling Relations for the Brush Thickness H in Various Regions of the Diagrams in Figures 2 and 3

NB	$v^{1/3}N\sigma^{-1/3}$	OrS, IS	$Nm^{-2/3}$
NC	$v^{1/5}N^{3/5}$	G	$N^{1/2}$
OsB	$Nm^{-1/2}$	SB	$N\sigma^{-1/3}m^{-2/3}\phi_s^{-1/3}$
PB	$N^3\sigma^{-1}m^{-2}$		

(indicated in the figure) are obtained by equating the expressions for the brush thickness in those two regimes, except for the OrS/IS boundary, which is obtained from the condition that the orientational energy of a polyion is of the order kT.[5,6] In the expressions given in the figure, v was omitted.

Above we described the scaling behavior of a brush (I) using the Gaussian expression for the stretching energy, (II) neglecting ternary and higher order interactions, and (III) using the mean-field approximation. In order to make a comparison with the numerical model, we have to simplify the picture slightly more, as we will do in Figure 3a. The limitations of the numerical approach used in the present paper, in particular the fact that it collects *inter-* as well as *intra*molecular interactions into one (averaged) mean field, cause it to break down at low densities. Here intermolecular interactions are negligible; as a consequence, also intramolecular interactions are neglected. The behavior of a single Gaussian coil with $H \simeq \sqrt{N}$ is recovered. In Figure 3a a modified diagram of a salt-free brush is shown, where the three regimes at low density (NC, OrS, and IS) are substituted by this *Gaussian* regime (G). This is the diagram that may be expected to agree with calculations from our numerical model. As is seen from Figure 3a, such a substitution makes the PB regime wider than in Figure 2. Correspondingly, the boundaries PB/G and NB/G are also shifted to higher values of σ.

So far we only considered brushes that are in contact with a salt-free solution. The effects of added salt have been described before.[2,4,16] We will summarize the main points of this analysis. The addition of electrolyte increases the screening of electrostatic interactions, and as a consequence a new regime appears between the OsB and PB regimes. This *salted brush* (SB) regime and the evolution of its boundaries upon further increase of the salt concentration are shown in Figure 3b,c. Below we will first describe the interactions in the SB regime and then discuss the location of its boundaries.

We adopt here the simple picture of a salted brush suggested in ref 2. According to this picture, when the concentration of salt ions exceeds by far the concentration of brush counterions, the brush characteristics are similar to those of a neutral brush. As mentioned before, we describe nonelectrostatic interunit interactions using a mean-field approximation and introduce $a^3v = a^3(1/2 - \chi)$ as the second virial coefficient of pair interactions. As will be derived below (eq 23), screened electrostatic interactions in the SB regime can be described by an *electrostatic* second virial coefficient a^3v_{el}, where[2,4]

$$v_{el} \cong \frac{1}{4\phi_s m^2} \tag{1}$$

and scaling relations can be obtained by substituting v_{el} for v in the expressions for a neutral brush (see Table 1).

We now turn to the size and shape of the SB regime. Upon increasing the salt concentration, beginning at $\phi_s = 0$, the SB regime will first appear next to the PB regime. The threshold salt concentration ϕ_s^0 above which salt effects become noticeable is given by the demand that the Debye screening length $\kappa^{-1} \simeq a\phi_s^{-1/2}$ is on the order of the brush thickness H. Since the maximal stretching of chains in the PB regime is attained at $m \simeq 1$, near the boundary with the OsB regime ($\sigma \simeq N^2$), one obtains $H \simeq N \simeq \phi_s^{-1/2}$ or $\phi_s^0 \simeq N^{-2}$. At $\phi_s < \phi_s^0$ the diagram of a brush coincides with that for a salt-free brush (Figure 3a). Increasing the salt content ($\phi_s > \phi_s^0$) results in the appearance of the SB

regime as indicated in Figure 3b; the highest point of this regime, located at the intersection of the lines $\sigma^2 m = \phi_s^{-2}$ and $\sigma m^{3/2} = N^2$, moves up along the latter line until the NB regime is reached at $\sigma = N$, $m = N^{2/3}$. At that point $\phi_s = N^{-4/3}$, which is the upper limit for Figure 3b.

If the salt concentration is further increased (Figure 3c), the horizontal boundary between the SB and NB regimes, at $m = \phi_s^{-1/2}$, moves down, thereby diminishing and narrowing the PB and OsB regimes. When m has decreased to the intersection of the lines $\sigma = N^{3/2}$ and $\sigma m^2 = N^{5/2}$, at $m^2 = N$ or $\phi_s = N^{-1}$, the PB regime has disappeared altogether. The effect of a further increase of ϕ_s (Figure 3d) is to enlarge the NB regime (to higher values of the charge density $1/m$), at the expense of the OsB and SB regimes.

Segment Density Profiles. The remainder of this section is devoted to a detailed description of the brush in the three high-density brush regimes: OsB, SB, and NB. First we derive a general description of the segment density profile, then we solve these equations neglecting excluded-volume interactions, and in the final part we derive an implicit equation for the profile with excluded-volume interactions taken into account.

In the OsB regime mobile counterions of charged chains are located mainly inside the brush. In the SB regime salt ions provide the screening of electrostatic repulsion between polycations. In both cases, the characteristic scale of smoothening of the counterion distribution in the brush and outer solution is given by the Debye–Hückel screening length:

$$\kappa^{-1} \simeq \begin{cases} am^{1/4}\sigma^{1/2} & \text{(OsB)} \\ a\phi_s^{-1/2} & \text{(SB)} \end{cases} \tag{2}$$

The expression for κ^{-1} in the OsB regime can be obtained from the conventional relation $\kappa \sim \sigma_s^{1/2}$, realizing that the screening of electrostatic interactions in this regime is carried out by the chain counterions with a concentration $N/(m\sigma H) \simeq \sigma^{-1} m^{-1/2}$. In the SB regime (where $\sigma_s \gg m^{-1/2}\sigma^{-1}$), the Debye length is determined by the external concentration ϕ_s.

If $\kappa^{-1} \ll Ha$, we can use the approximation of local electroneutrality. This results in a considerable simplification of the description of the system, because it permits us to reduce all electrostatic interactions (if we neglect free energy contributions due to correlation effects[3,4]) to the translational entropy of (counter)ions only. Following the scheme of ref 3, we first generalize the results of ref 4 and take nonelectrostatic volume interactions between units as well as the volume of salt ions into account. For simplicity we assume that the volume of an ion coincides with that of a polymer unit, a^3. Denoting by $\phi_p(x)$ the volume fraction of polymer segments at distance ax from the grafting surface and with $\phi_+(x)$ and $\phi_-(x)$ the corresponding profiles of co-ions and counterions, respectively, we write the condition of local electroneutrality in the brush as:

$$\phi_p(x)/m + \phi_+(x) = \phi_-(x) \tag{3}$$

We keep in mind that all concentrations are a function of the position in the brush and omit x from the equations. Note that both ϕ_+ and ϕ_- converge to the bulk solution concentration ϕ_s outside the brush ($x \to \infty$). Assuming that contact interactions are identical for solvent and ions, we can write the local free energy density in a brush as:

$$\frac{f[\phi_+,\phi_p]}{kT} = \phi_+ \ln \phi_+ + \phi_- \ln \phi_- + \phi_0 \ln \phi_0 + \chi\phi_p(1-\phi_p) \tag{4}$$

where ϕ_- can be expressed in ϕ_+ and ϕ_p through eq 3. The volume fraction of solvent, ϕ_0, follows from:

$$\sum_i \phi_i = \phi_p + \phi_+ + \phi_- + \phi_0 = 1 \tag{5}$$

The first two terms in eq 4 take into account the translational entropy of salt co-ions and counterions, respectively, the third term represents the translational entropy of solvent molecules (i.e., excluded-volume effects), and the last term accounts for the solvent quality (χ is the familiar Flory–Huggins parameter[17]). In the bulk solution, where $\phi_p = 0$ and $\phi_+ = \phi_- = \phi_s$, the free energy is given by:

$$\frac{f^b[\phi_s]}{kT} = 2\phi_s \ln \phi_s + (1-2\phi_s)\ln(1-2\phi_s) \tag{6}$$

Following the scheme of ref 3, the conditions for equilibrium in a brush are given by:

$$\frac{\delta f[\phi_+,\phi_p]}{\delta \phi_+} = \mu_s = \frac{\partial f^b[\phi_s]}{\partial \phi_s} \tag{7}$$

$$\frac{1}{kT}\frac{\delta f[\phi_+,\phi_p]}{\delta \phi_p} = \Lambda - \frac{3\pi^2}{8N^2}x^2 \tag{8}$$

where μ_s is the chemical potential of salt and Λ is an undetermined constant providing normalization of the profile of polymer units. Equation 7 reflects the constancy of the salt chemical potential inside and outside the brush, while eq 8 is analogous to that for a one-component brush.[9] The derivation of eq 8 was obtained along the lines of ref 18 from a first approach by Semenov.[19] It is briefly outlined in the appendix. The two approximations used are that the elastic free energy of stretching is given by a Gaussian expression and that the full set of conformations is reduced: all conformations having their end segments at the same distance x' from the surface are represented by only one conformation. After some algebra one obtains

$$\frac{(\phi_+ + \phi_p/m)(\phi_+)}{[1-2\phi_+ - \phi_p(1+1/m)]^2} = \frac{(\phi_s)^2}{[1-2\phi_s]^2} \tag{9}$$

$$\frac{(\phi_+ + \phi_p/m)}{[1-2\phi_+ - \phi_p(1+1/m)]^{1+m}} = \frac{\phi_s \exp[(H^2-x^2)/h_0{}^2 + 2\chi\phi_p m]}{[1-2\phi_s]^{1+m}} \tag{10}$$

where H is the upper boundary of the brush, determined by the normalization condition:

$$\sigma\int_0^H \phi_p(x)\,dx = N \tag{11}$$

and $h_0 a$ is the decay length of the (Gaussian) segment density profile of the corresponding salt-free brush, given

by:

$$h_0^2 = \frac{8}{3\pi^2}\frac{N^2}{m} \tag{12}$$

The simultaneous solution of eqs 9–11 provides the equilibrium parameters of a polyelectrolyte brush: its height, H, the profile $\phi_p(x)$ of polymer units, and the distributions of salt co-ions $\phi_+(x)$ and counterions $\phi_-(x) = \phi_+(x) + \phi_p(x)/m$.

Profiles. No Excluded Volume. If nonelectrostatic excluded-volume effects are totally neglected, these equations transform into the corresponding equations of ref 3:

$$\phi_+(x) = \phi_s \exp[-(H^2 - x^2)/h_0^2] \tag{13}$$

$$\phi_p(x) = m(\phi_s^2/\phi_+(x) - \phi_+(x)) \tag{14}$$

The upper boundary of the layer, H, is determined by the normalization condition (11, 13, 14):

$$\gamma = e^{z^2}\int_0^z e^{-t^2}\,dt - e^{-z^2}\int_0^z e^{t^2}\,dt \tag{15}$$

with

$$z = H/h_0 \tag{16}$$

$$\gamma = N/m\sigma h_0\phi_s \tag{17}$$

Here we introduce two dimensionless parameters that will prove to be convenient: a rescaled layer thickness $z = H/h_0$ and γ, which is the ratio between the concentration of counterions in the corresponding salt-free brush $N/m\sigma h_0$, and the counterion concentration ϕ_s in the actual bulk solution. In a salt-free brush γ is large, decreasing as ϕ_s becomes higher. For a salted brush γ is smaller than unity. The analysis of eq 15 shows that, depending on the value of γ, several regimes can be distinguished, which will be discussed shortly. Starting at low salt concentrations, where the second term in eq 15 may be neglected, it can be easily seen that, when ϕ_s goes to zero, $z = H/h_0$ must go to infinity as

$$z \approx \left[\ln\left(\frac{2}{\sqrt{\pi}}\gamma\right)\right]^{1/2} \tag{18}$$

In the limit of a salt-free case, $\phi_s = 0$ (*osmotic brush*), the distribution of polymer units in a brush is given by[3]

$$\phi_p(x) = \frac{2}{\sqrt{\pi}}\frac{N}{\sigma h_0}e^{-x^2/h_0^2} \tag{19}$$

Introducing the weight-averaged brush thickness, defined as:

$$H_{rms}^2 = \frac{\int_0^H \phi_p(x)\,x^2\,dx}{\int_0^H \phi_p(x)\,dx} \tag{20}$$

as a convenient measure of brush thickness, we find that it is given by:

$$H_{rms}^2 = \frac{1}{2}h_0^2 \tag{21}$$

Now let us consider the case of a considerable amount of salt in solution, leading to $z \ll 1$ (*salted brush*). The expansion of the integrals in eq 15 with respect to small parameters z transforms it into

$$\gamma \approx (4/3)z^3 \tag{22}$$

Substitution of h_0 from eq 12 into the definition of γ (eq 17) then gives

$$H \approx N\left(\frac{8v_{el}}{\pi^2\sigma}\right)^{1/3} \tag{23}$$

where v_{el}, given by eq 1, is the electrostatic excluded-volume parameter. Other characteristics are given by:

$$\phi_p(x) \approx \frac{3}{2}\frac{N}{\sigma H}(1 - x^2/H^2) \tag{24}$$

$$H_{rms}^2 \approx (1/5)H^2 \tag{25}$$

$$\phi_+(x) \approx \phi_s[1 - (H^2 - x^2)/h_0^2] \approx \phi_s \tag{26}$$

Thus, in a salt-dominance regime ($\gamma \ll 1$) the electrostatic interactions in a brush can be described by an electrostatic excluded-volume parameter v_{el} and the brush characteristics are similar to those of a neutral brush, with v_{el} substituted for v.

Profile. Excluded Volume. In the previous paragraph all nonelectrostatic excluded-volume effects in the system were ignored. As was already mentioned above, expression (4) takes into account the volume of all ions and polymer units through the mixing entropy. However, in many practical cases, the volume of the ions can be neglected with respect to the volume of the polymer units. Neglecting the contribution of the ions in expression (5) and using once again the conditions of equilibrium (eqs 7 and 8), one obtains

$$\phi_+(x) = \phi_s \exp\{-(H^2 - x^2)/h_0^2 + m[\ln(1 - \phi_p) + 2\chi\phi_p]\} \tag{27}$$

$$\frac{\phi_p(x)}{m\phi_s} = \exp\{(H^2 - x^2)/h_0^2 + m[\ln(1 - \phi_p) + 2\chi\phi_p]\} - \exp\{-(H^2 - x^2)/h_0^2 - m[\ln(1 - \phi_p) + 2\chi\phi_p]\} \tag{28}$$

Under the conditions of salt dominance ($z \ll 1$) and for not too dense layers ($\phi_p \ll 1$), a virial expansion of the mixing entropy in z and ϕ_p is justified and an approximate solution of eq 28 is available. We arrive at the same expressions that were derived for the osmotic brush (eqs 23 and 24) although now we have to substitute an *effective* excluded-volume parameter v_{eff} for v_{el}, given by

$$v_{eff} = v + v_{el} \tag{29}$$

Hence, v_{eff} consists of the excluded-volume part $v = 1/2 - \chi$, for uncharged units, and an electrostatic part v_{el}, given by eq 1. At considerable salt contents $v_{el} \ll v$ and the nonelectrostatic interactions between units dominate over electrostatic ones: the polyelectrolyte brush passes into the quasi-neutral regime. The structure of a neutral brush is well-known:[20–22] in a good solvent, the segment density profile and the brush thickness are given by relations (24) and (25), where H is obtained from eq 23 with v_{eff} substituted for v_{el}.

For relatively dense brushes, when the virial expansion of the mixing entropy breaks down and the volume of salt ions can be essential, the equation for the profile $\phi_p(x)$ can be obtained implicitly only. Solving eq 9 for ϕ_+ and

substituting the result into eq 10, one obtains for the good solvent case ($\chi = 0$):

$$\exp\left(\frac{H^2 - x^2}{h_0^2}\right) = \frac{(1-2b)^m}{2b[1-\phi_p - c]^{m+1}} \times [\phi_p(1-4b^2)/m - 4b^2(1-\phi_p) + c] \quad (30)$$

where

$$b = \phi_s/(1-2\phi_s)$$

$$c^2 = \frac{\phi_p}{m^2}(1-4b^2) + 4b^2(1-\phi_p)^2$$

The right-hand part of eq 30 can be viewed as a rescaled volume fraction $\mathcal{F}(x)$. It follows from the left-hand side that, if we plot $\mathcal{F}(x)$ on a logarithmic scale as a function of x^2/h_0^2, we may expect to find a straight line with slope -1 and intercept H^2/h_0^2. We shall use eq 30 later for a detailed comparison of the analytical predictions with results of the numerical SCF theory.

Note that in the limit of a noncharged brush ($m \to \infty$) eq 30 reduces to

$$\phi_p(x) = 1 - e^{-K^2(H^2-x^2)} \quad (31)$$

where $K^2 = 3\pi^2/(8N^2)$ and H is obtained from eq 11, which has to be solved numerically. Expression (31) has been derived before[22] and is slightly more precise than the more well-known parabola given by eq 24. It reduces to the parabola at low densities.

III. Self-Consistent-Field Lattice Model

General Procedures. The self-consistent-field (SCF) lattice model initially developed by Scheutjens and Fleer for the adsorption of homopolymers[10,11] serves as the starting point of our numerical analysis. The model contains a number of simplifying assumptions. First, the mean-field approximation implies the replacement of the local potential $u(x,y,z,t)$ of a segment at position (x, y, z) and time t by a time-independent potential $u(x)$ for a segment at a distance x from the surface. Hence, a preaveraging over the variables y, z, and t is carried out. Second, for the generation of conformations a first-order Markov approximation is used: the position of any segment is restricted by the position of its immediate neighbors along the chain only (i.e., backfolding is allowed). The electrostatic interactions are handled using the multilayer Stern model,[14] which is a straightforward modification of the Poisson–Boltzmann equation to the case of a lattice containing an arbitrary mixture of molecules, taking into account the volume of polymer, solvent, and salt molecules. The introduction of a lattice, finally, is convenient to define and count conformations.

A major drawback of the model is the fact that the resulting equations can only be solved numerically; exact analytical expressions cannot be obtained. Despite these shortcomings, there are two very important reasons to use the model. First, many characteristics of the system, including profiles of all molecules and all thermodynamic properties of the system, may be obtained. Second, these properties are calculated without any presupposition as to the conformations of the polymers.

Potential Field. We divide the half-space next to a surface in parallel layers, numbered $x = 1, ..., M$ where M is sufficiently large. The potential experienced by a segment depends on its position x only. In the absence of chemical interactions ($\chi = 0$), the potential energy of a segment of type A in layer x is given by[13,14]

$$u_A(x) = u'(x) + eq_A\psi(x) \quad (32)$$

where $u'(x)$ is a Lagrange multiplier for layer x, introduced to meet the constraint that the lattice is completely filled:

$$\sum_A \phi_A(x) = 1 \ (x = 1, ..., M) \quad (33)$$

This summation runs over all segment types in the system: the brush segments (p), co-ions (+), counterions (−), and solvent molecules (0).

The last term of eq 32 represents the electrostatic contribution to the potential energy of a segment. In this term, e is the elementary charge, q_A the valence of a segment A (zero for the solvent, +1 for the cations, −1 for the anions, and $1/m$ for the polymer segments). A variation of m could, in principle, be carried out by inserting uncharged segments between the fully charged segments. This would preclude, however, a continuous variation of m. Therefore, we choose to give evergy segment a charge qe, where $0 \lesssim q \lesssim 1$. Note that, as a consequence, the brush molecules are homopolymers. The electrostatic potential $\psi(x)$ in each layer x is obtained from the set of equations:

$$\frac{\partial^2\psi(x)}{\partial x^2} = \frac{\rho(x)}{\epsilon(x)}d^2 \ (x = 1, ..., M) \quad (34)$$

In this equation the lattice spacing d is needed to keep x dimensionless. In our lattice calculations we use a discrete analogue of eq 34, taking into account the changes in dielectric permittivity between different layers.[14] The space charge density $\rho(x)$ in layer x and the dielectric permittivity $\epsilon(x)$ of layer x are obtained from the following mean-field expressions, in which ϵ_A is the dielectric permittivity of pure A and $V_{cell} = d^3$ (cubic lattice) is the volume of one lattice cell:

$$\rho(x) = \frac{\sum_A q_A e \phi_A(x)}{V_{cell}} \quad (35)$$

$$\epsilon(x) = \sum_A \epsilon_A \phi(x) \quad (36)$$

The electroneutrality of the system is ensured by setting the field strength at the boundaries zero:

$$\left.\frac{\partial\psi}{\partial x}\right|_{x=0} = \left.\frac{\partial\psi}{\partial x}\right|_{x=M} = 0 \quad (37)$$

Again, in the lattice model a discrete version of these expressions is used.[14]

Segment Density Profile. In order to calculate the volume fraction profile, we introduce a function $G_A(x,s|x',s')$, which is the combined statistical weight of all conformations of chain parts of molecules of type A starting with segment s' in layer x' and ending with segment s in layer x. Summation of $G_A(x,s|x',1)$ over all x' leads to the end-point distribution function $G_A(x,s|1)$ of a sequence 1, 2, ..., s. It is convenient to define a weighting factor for species A as

$$G_A(x) = e^{-u_A(x)/kT} \quad (38)$$

Now we have for grafted chains, which have their first

segment restricted to the first layer:

$$G_p(x,1|1) = \begin{cases} G_p(x) & (x = 1) \\ 0 & (x > 1) \end{cases} \quad (39)$$

and similarly

$$G_p(x,N|N) = G_p(x) \qquad \text{for any } x \quad (40)$$

where N is the number of segments of the molecule. The solvent and salt molecules are assumed to consist of only one segment ($N_0 = N_- = N_+ = 1$). Thus we have, e.g., for the co-ions, $G_+(x,1|1) = G_+(x,N|N) = G_+(x)$ for all values of x.

The first-order Markov approximation allows us to obtain a simple recurrence relation to compute the distribution function $G_p(x,s+1|1)$ from its predecessor $G_p(x,s|1)$ by taking into account all possible steps from segment s to $s+1$, regardless of the positions of all segments 1 to $s-1$:

$$G_p(x,s+1|1) = G_p(x)\,\langle G_p(x,s|1)\rangle \quad (41)$$

where $\langle G_p(x,s|1)\rangle$ is a shorthand notation for $G_p(x,s|1)$ averaged over the neighbors (in layers $x-1$, x, and $x+1$) of a lattice site in layer x. Applying expression (41) recursively $N-1$ times to the starting relation (39) and also $N-1$ times to expression (40), two sets of N distribution functions are generated. From these sets many characteristics of the adsorbed layer can be calculated. For the brush molecule, the volume fraction profile is given by:

$$\phi_p(x) = C_p \sum_{s=1}^{N_p} \frac{G_p(x,s|1)\,G_p(x,s|N)}{G_p(x)} \quad (42)$$

where $C_p = \theta_p/N_pG_p(N|1)$ is the proper normalization factor to fix the total amount θ_p of polymer on the surface, where θ_p is defined as $\theta_p = \sum_x \phi_p(x)$ and

$$G_p(N|1) = \sum_{x=1}^{x=M} G_p(x,N|1) \quad (43)$$

The area σ per chain, used in the analytical model (section II), is obtained as $\sigma = N/\theta$.

The volume fraction profile for the salt and solvent molecules, which are in full equilibrium with those far away from the surface (the bulk solution), is simply given by:

$$\phi_A(x) = \phi_A{}^b G_A(x) \quad (44)$$

where A = + (co-ion), − (counterion), or 0 (solvent).

Numerical Solution. We now have for any monomer type A in every layer x two unknowns $\phi(x)$ and $G(x) = e^{-u(x)/kT}$ and two corresponding equations: 32 and 42 or 44. Additionally we have for every layer two unknowns $\psi(x)$ and $u'(x)$ with corresponding eqs 33 and 34. This set of equations can be solved numerically.

IV. Results

Parameters. In this section we present numerical results from the lattice model (section III) and discuss them in terms of the analytical model (section II). We vary the chain length N, the area per chain σ (=the inverse anchoring density), the average distance m between two charges on the brush molecules (=the inverse charge density), and the salt concentration ϕ_s and examine the effect on the brush (root-mean-square) thickness H_{rms} as well as the segment density profiles. Variation of m is carried out by giving every segment a charge qe, where $0 \lesssim q \lesssim 1$. A chain for which $q = 0.1$ is equivalent to a chain with $m = 10$. We use a cubic lattice with a lattice constant $d = 0.6$ nm. The relative permittivity of the solvent (water) is chosen as $\epsilon_r = 80$; the permittivity of the other substances (surface, polymer, and salt molecules) is taken as $\epsilon_r = 5$. The solvent is taken to be a good solvent for the polymer ($\chi = 0$). Calculations for poor solvents are possible, in both the analytical and numerical models, and should lead to a collapse of the polyelectrolyte brush; we defer the discussion of these systems to a following paper.

Scaling Picture. Figure 4a shows the diagram of states for a charged brush with $N = 500$, in a low concentration of salt ($\phi_s = 10^{-4}$). This salt concentration corresponds to $N^{-1.48}$, which is in between the limits $N^{-4/3}$ and N^{-2}, and so Figure 3b applies. To compare Figure 4a with the results of the lattice model, we calculated the dependence of the brush thickness H_{rms} on each of the parameters σ, m, and N throughout the parameter space, denoting the exponents with α_σ, α_m, and α_N, respectively ($H \sim \sigma^{\alpha_\sigma} m^{\alpha_m} N^{\alpha_N}$). For example, assuming a power law dependence of H on σ, the exponent α_σ of this power law is found from:

$$\alpha_\sigma = \frac{\partial \log H}{\partial \log \sigma} \quad (45)$$

Obviously, we use a discrete version of this equation, $\Delta\sigma/\sigma$ being on the order of 10%. In this way exponents are calculated for the power law dependence of the thickness on the area σ per chain (Figure 4b), the charge separation m (Figure 4c), and the chain length N (Figure 4d). The exponents are displayed using contour plots, where the isolines connect points of equal values. These values may be compared with the analytical predictions for the various regimes (Table 1), which are indicated in the rectangular boxes in the four diagrams of Figure 4.

Inspection of Figure 4b reveals the four major regimes in Figure 4a: $\alpha_\sigma = 0$ for G and OsB, $\alpha_\sigma = -1/3$ for SB and NB. At extremely low σ and high m (upper left corner in Figure 4b) an even lower exponent $\alpha_\sigma < -0.40$ is found. This is due to the onset of ternary and higher interactions, which were neglected in the derivation of the $-1/3$ power law.

The slope of the contour lines should follow roughly the slope of the corresponding boundaries between the two neighboring regimes. This seems to be the case for the NB/G, OsB/SB, and SB/G boundaries, but a deviation can be seen for the NB/OsB boundary at low σ. Probably this is due to the onset of higher order interactions as well.

In Figure 4c the correct power law exponent $\alpha_m = 0$ for the NB and G regimes can be recognized and an exponent close to $\alpha_m = -2/3$ for the SB regime is found. For the OsB regime the numerical model seems to give a somewhat too low exponent, around $\alpha_m \approx 0.40$.

For the dependence of σ on N (shown in Figure 4d) we find the correct exponent $\alpha_N = 0.5$ in the Gaussian and $\alpha_N = 1.0$ in the osmotic and neutral brush regimes but an exponent slightly above unity (≈ 1.1) at the transition between the SB and G regimes. This small deviation may be reminiscent of the Pincus regime (where α_N should be 3).

In the results of Figure 4 as discussed above, we find good agreement between the numerical and analytical predictions on the power law behavior in OsB, NB, SB, and G regimes. The one regime that is not easily recognized in these diagrams is the Pincus brush regime (PB). This

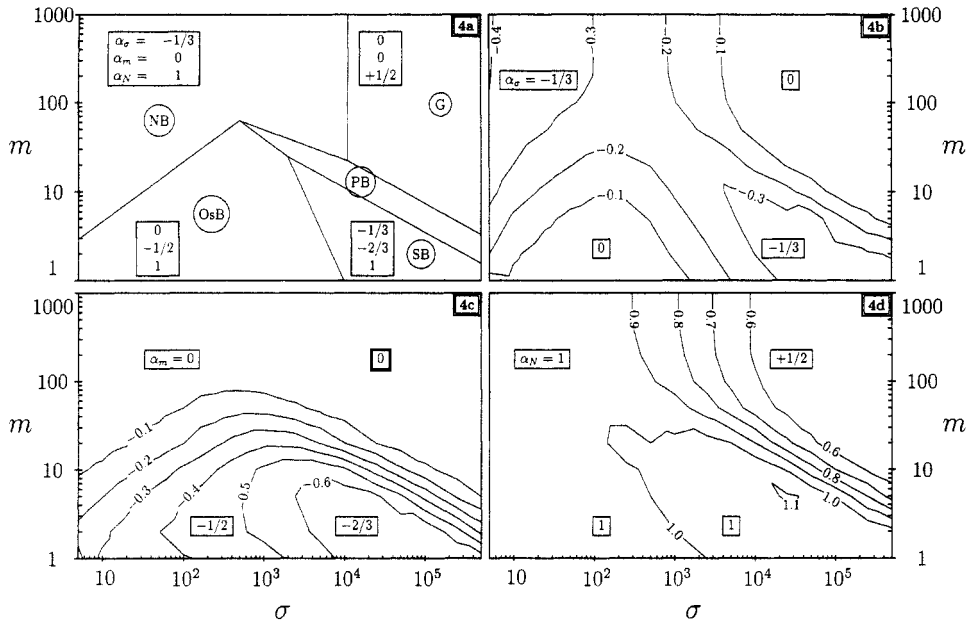

Figure 4. Diagram of states for a polymer with chain length $N = 500$ at a salt concentration $\phi_s = 10^{-4}$ (a) and two-dimensional contour plots calculated using the SCF model giving the value of the exponent α_σ for the power law dependence of H on σ (b), the exponent α_m (c), and α_N (d). Values of the isolines are indicated, as well as the analytical predictions for the exponents in each of the regimes (in the rectangular boxes).

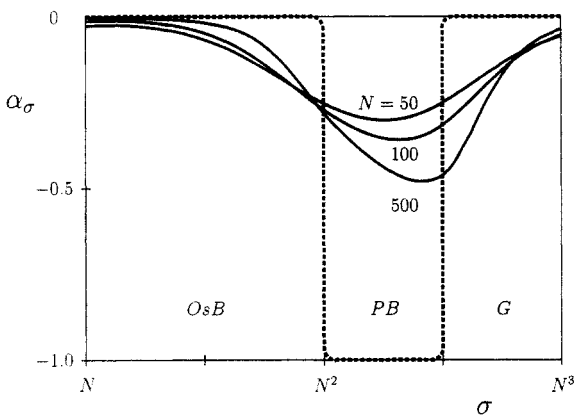

Figure 5. Exponent α_σ for the dependence of the brush thickness on the area σ per chain (i.e., $H_{rms} \sim \sigma^\alpha$), as a function of σ for three different chain lengths (indicated) at salt concentrations $\phi_s = N^{-2}$. The calculations with the SCF theory are represented by the continuous curves; the prediction of the analytical theory is shown as the dashed curve.

is not quite unexpected, since for our choice of chain length $N = 500$ the transitions between the various regimes are relatively broad, and at the salt concentration $\phi_s = 10^{-4}$ the PB regime is very narrow. To make this transition sharper, the chain length should be increased, and to make the PB regime wider, a lower salt concentration is needed. However, due to convergence problems, there is a lower limit on salt concentrations that can be reached. For our present software this limit is located around $\phi_s \approx 10^{-5}$.

To illustrate the difficulties encountered when trying to find the PB regime, we present in Figure 5 results of calculations that were aimed specifically at investigating this peculiar regime. We consider a system at $m = 1$, where the PB regime is widest, and plot α_σ as a function of σ. The salt concentration was adjusted to the chain length according to $\phi_s = N^{-2}$, so that Figure 3a should apply. Thus we may expect the SB regime to be absent, and any deviation from $\alpha_\sigma = 0$, which is valid in the neighboring OsB and G regimes, must be due to the onset of the PB regime, where a value $\alpha_\sigma = -1.0$ is expected. This analytical prediction for α_σ is indicated by the dashed curve in Figure 5. The three continuous curves correspond to numerical calculations for three different chain lengths (length indicated).

The minimum in α_σ decreases with N and is already for $N = 500$ clearly lower than the value $\alpha_\sigma = -1/3$, which is the lowest value in any of the other theoretical regimes. In other words, a regime with $\alpha_\sigma \ll -1/3$, probably corresponding to a kind of PB regime, can be predicted with a mean-field theory. The exact power law for this regime cannot be found with our present computer program, since it requires calculations at very high chain lengths and extremely low salt concentrations. Note, however, that the present numerical limits of the SCF model are of the same order as physical limits in real systems. Therefore, the existence of the PB regime, although interesting for theoreticians, will be hard to prove experimentally as well. Note that our mean-field assumption already causes the Pincus regime to be wider than in more exact treatments (compare Figures 2 and 3).

Above we considered the general scaling behavior of the thickness in the full parameter space. Below we will inspect more carefully the OsB/NB transition (upon increasing m) and the OsB/SB/NB transition (upon increasing ϕ_s).

The transition from the OsB to the NB regime is illustrated in Figure 6, where we plot the brush thickness as a function of m for three anchoring densities (indicated), using $\phi_s = 10^{-5}$ and otherwise the same parameters as used in Figure 4. Actually, Figure 6 can be compared to a vertical cross section in Figure 4 at the indicated values for σ. At high charge density ($m < 10$), we find the OsB regime with hardly any dependence on σ and a power law dependence on m with almost the analytically predicted exponent $\alpha_m = -0.5$ (indicated by the dashed line). Careful inspection shows the slope (and thus the exponent) to decrease slightly at extremely high charge densities ($m < 2$). This may be attributed to the finite extensibility of the chains, i.e., the breakdown of the Gaussian expression for the chain elasticity. At low charge density ($m > N^{4/3}\sigma^{-2/3}$), on the other hand, we find the NB regime with little or no dependence on m but with a big effect of the anchoring density.

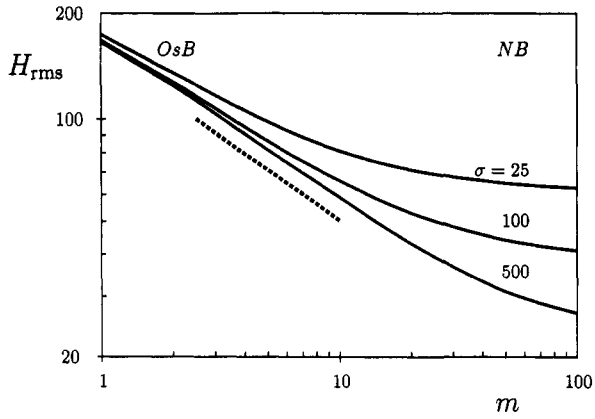

Figure 6. Brush thickness H_{rms} as a function of the inverse charge density m, for three different values of the area σ per chain. Parameters: $N = 500$, $\phi_s = 10^{-5}$. The slope $-1/2$ on the double-logarithmic plot, as expected in the OsB regime, is indicated by the dashed line.

As an introduction to Figure 7, let us take a look at Figure 3a–d again and consider specifically a brush corresponding to one σ, m coordinate (e.g., $\sigma = N$, $m = N^{0.5}$). At low ϕ_s (Figure 3a,b), such a brush finds itself in the OsB regime. Upon increasing the salt concentration above $\phi_s = \sigma^{-1}m^{-1/2}$, it will be located first in the SB regime (Figure 3c) and finally, above $\phi_s = m^{-2}$ in the NB regime (Figure 3d). This OsB → SB → NB transition is illustrated in Figure 7a,b. First, we plot the thickness of a brush as a function of the salt concentration (increasing from right to left) for two charge densities ($m = 1$ and 10), each at two different anchoring densities ($\sigma = 25$ and 500). At low salt concentrations, the systems for $\sigma = 500$ and that for $m = 1$, $\sigma = 25$ are in the OsB regime. As the salt concentration is increased, these three systems enter the SB regime, crossing the OsB/SB boundary around $\phi_s = \sigma^{-1}m^{-1/2}$, which value is indicated in Figure 7a by the upward arrows. Indeed around these points H_{rms} starts to decrease with the salt concentration, and for the system with $m = 10$ eventually the SB/NB boundary is crossed at $\phi_s = 1/m^2$ (indicated by a solid triangle), leading to a thickness that should not depend on either ϕ_s or m.

The fourth curve in Figure 7a represents the system $m = 10$, $\sigma = 25$. This brush is located at the OsB/NB boundary at low ϕ_s and passes directly into the NB regime with increasing salt concentration. Consequently, its thickness is hardly effected by any change in ϕ_s.

When we substitute $v_{eff} = v + v_{el}$ (eq 29) for v_{el} in eq 23, we have an equation that incorporates electrostatic as well as nonelectrostatic excluded-volume interactions. Consequently, this equation should describe the effect of increasing ϕ_s in the SB regime, as well as in the SB/NB transition region. This is checked in Figure 7b, where we plot the same data as in Figure 7a, rescaled according to these equations in such a way that a straight line with slope $1/3$ is expected for the points corresponding to the SB regime. Indeed we find that the data for different charge and anchoring densities can be collected onto one master curve, as long as they describe a system in the SB or NB regime (low v_{eff}, high ϕ_s). Each of the four curves eventually branches off as, for high v_{eff} or low ϕ_s, it reaches the OsB regime, where eq 23 is no longer valid and the brush thickness becomes independent of ϕ_s (see Table 1). The level of this plateau at high v_{eff} (which is the same plateau as that for low ϕ_s in Figure 7a) scales as $m^{-1/2}$, as expected from Table 1.

Segment Density Profiles. In Figures 4–7 we checked the scaling dependencies for the brush thickness. Now we turn to the shape of the segment density profiles.

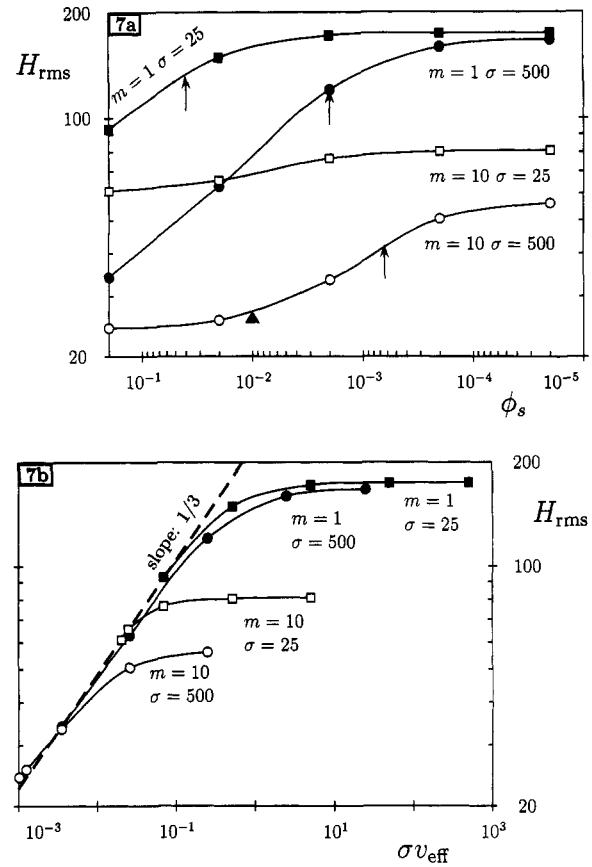

Figure 7. (a) Brush thickness H_{rms} as a function of the salt concentration ϕ_s, for four different combinations of σ and m (indicated) and $N = 500$. The salt concentrations $\phi_s = \sigma^{-1}m^{-1/2}$, corresponding to the OsB/SB transitions, are indicated by the upward arrows; the concentration $\phi_s = m^{-2}$, representative for the SB/NB transition of the $m = 10$, $\sigma = 500$ brush, is given as a solid triangle. (b) The same data as in Figure 7a, plotting $\sigma^{-1}v_{eff}$ (see eqs 1 and 29) instead of ϕ_s on the horizontal axis. Such a plot leads to a linear dependence with slope $1/3$ (dashed line) for the part of the curve corresponding to the SB regime, followed by a plateau in the OsB regime.

Analytical predictions for the profile of a polyelectrolyte brush are based on the assumption of local electroneutrality in the OsB and SB regimes. Figure 8a shows the profile of total positive charge $\phi_+ + \phi_p/m$ as a function of x for a brush in the OsB regime. The dotted curve corresponds to the profile ϕ_- of mobile counterions. Both profiles coincide nearly completely, thus confirming eq 3 (i.e., the assumption of local electroneutrality).

Figure 8a presents also the dependence of the dimensionless electrostatic potential $y(x)$, defined as $e\psi(x)/kT$. As can be seen from Figure 8, $\psi(x)$ is evidently a nonlinear function of x within the brush. This nonlinearity of the potential profile enforces (through Poisson's law, eq 34) deviations from the local electroneutrality. However, this differential charge density is much smaller than the absolute value of positive (or negative) charge in the brush. It is not seen on the scale of Figure 8 except for a small region close to the surface. Thus, the condition (3) of local electroneutrality is, indeed, a reasonable approximation for describing the internal brush structure in the OsB regime. The deviations are even smaller (not shown) in the SB regime. We note that it is possible to obtain the electrostatic potential profile from the analytical model, by first solving eqs 27 and 28 for the profile $\phi_+(x)$ and applying $y(x) = -\ln[\phi_+(x)/\phi_s]$. It is found to agree approximately with the results of the numerical model.

A complete breakdown of the local electroneutrality is expected outside the OsB and SB regimes. This is

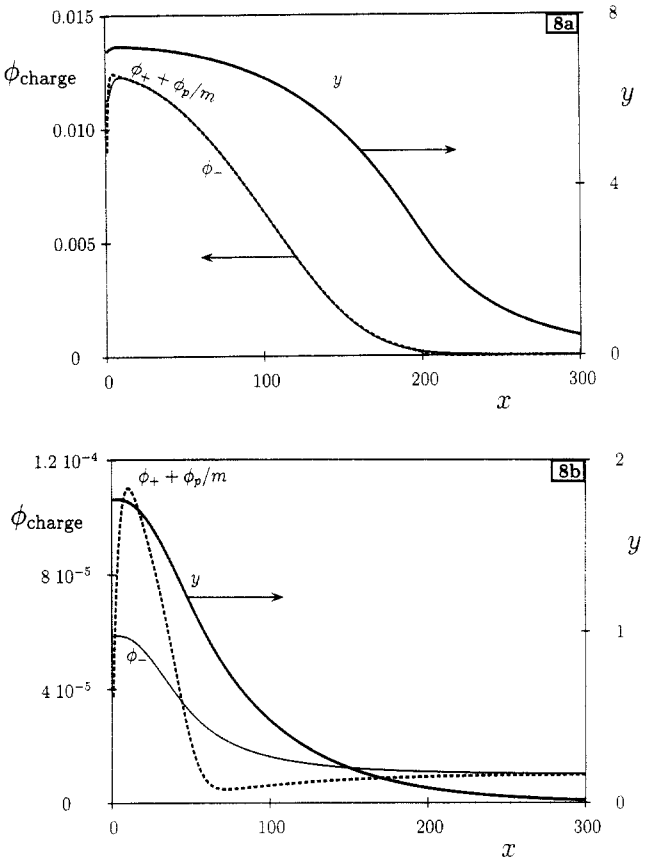

Figure 8. Density profiles of positive charge ($\phi_p/m + \phi_+$), and negative charge (ϕ_-), and the profiles of the dimensionless electrostatic potential ($y = e\psi/kT$) for an osmotic brush (a) and a Pincus brush (b). Parameters: $N = 500$, $\sigma = 40$, $m = 10$, $\phi_s = 10^{-5}$ (a) and $N = 500$, $\sigma = N^{1.4} \approx 6000$, $m = N^{-0.5} \approx 0.045$, $\phi_s = 10^{-5}$ (b).

illustrated in Figure 8b, where we plot the same three quantities as in Figure 8a, but now for a brush that is (according to the analytical theory) located in the PB regime. We find, indeed, a considerable difference between the profiles of positive and negative charge. Note that only at the intersection point of these charge profiles ($x \approx 50$) the system is locally electroneutral. Consequently, at this point the curve representing the electrostatic potential y shows an inflection point. While illustrating the breakdown of local electroneutrality, this diagram also shows why the PB scaling relations are not recovered. The basic assumption leading to the PB regime is that all counterions leave the brush. This is clearly not the case in the example: more than 50% of the brush charge is compensated by counterions that are located within the brush.

Since the local electroneutrality condition is fulfilled in the OsB and SB regimes, we expect the segment density profiles to obey the predicted dependences as discussed above. In Figure 9a we plot the segment density profiles for a charged brush ($N = 500$, $\sigma = 40$, $m = 10$) at high ($\phi_s = 10^{-2}$), intermediate ($\phi_s = 10^{-3}$), and low ($\phi_s = 10^{-5}$) salt concentrations. According to the diagrams of Figure 3, at the high salt concentration the brush is in the quasi-neutral brush regime (NB) and at the lower salt concentration in the osmotic brush regime (OsB), whereas at the intermediate concentration the salted brush regime (SB) applies.

In the quasi-neutral brush regime, the profile of a polyelectrolyte brush is expected to coincide with that for a neutral brush. In a good solvent and at low grafting density, when only pair contacts between units are significant, the segment density profile is parabolic.[21] However, in order to make the comparison with the numerical results more precise, we use the more general expression (31) which takes into account also higher order interactions. Thus, plotting the calculated distribution of polymer segments in the brush as $\ln[1 - \phi_p(x)]$ vs $(x/H)^2$, one expects a straight line. As is seen from Figure 9b, the profile corresponding to the highest salt concentration turns indeed into a straight line in such a representation. However, the thickness is still slightly higher than that of an uncharged chain, which reaches $\phi_p = 0$ exactly at $x = H$.

For a charged brush in the OsB regime, an analytical expression for the density profile is given by eq 19, provided that all nonelectrostatic interactions are neglected. From this equation a straight line is expected, when the profile is plotted as $\ln \phi_p$ vs $(x/h_0)^2$. This plot is shown in Figure 9c, where, to a first approximation, a more or less straight line is seen for the profile corresponding to the lowest salt concentration. The substantial deviation from the straight line must be attributed to the neglect of nonelectrostatic excluded-volume interactions.

Finally, we use the general eq 30 for the representation of the profiles. Doing so, we take into account both electrostatic and nonelectrostatic interactions between grafted polycations, salt co-ions, and all counterions. Plotting the profiles as $\ln \mathcal{J}(\phi_p)$ vs $(x/h_0)^2$, where $\mathcal{J}(\phi_p)$ is given by the right-hand side of eq 30, we obtain straight lines for all three (NB, SB, and OsB) profiles with the same slope −1. The intercept $\mathcal{J}(x=0)$ can, according to eq 30, be used to calculate the brush thickness H:

$$H^2 = h_0^2 \ln[\mathcal{J}(x=0)] \tag{46}$$

This thickness increases to infinity when the salt concentration goes to zero (compare eq 18).

Thus, in spite of the fact that an exact analytical expression for the segment density profile is not available from eq 30, it does predict rescaled coordinates in which the density profiles of polyelectrolyte brushes with various values of N, σ, m, and ϕ_s are transformed into straight lines with a slope −1.

Deviations from these straight lines, however, are noticeable. In the OsB regime ($\phi_s = 10^{-5}$), the downward deviation of the actual density profile from the analytical prediction is due to the finite extensibility of grafted chains.

At higher salt concentrations deviations appear in the opposite direction: the numerical SCF theory predicts a more extended profile than that predicted by the analytical theory. This deviation is due to fluctuations at the edge of the brush. These fluctuations are not found in the analytical theory due to the replacement of all conformations having the free end at $x = x'$ by one (the most probable) conformation. This replacement effectively discards conformations that turn back in the direction of the surface. The deviation (smoothening of the profile near the periphery of the brush) is expected to increase with diminishing brush thickness (increasing salt content). However, on the scale of Figure 9d, this increase is hardly noticeable.

V. Conclusions

In this paper we compare the analytical predictions on the structure and scaling relations of a charged brush[3,4] with a numerical lattice model.[12] Both models are self-consistent-field (SCF) methods. The analytical model classifies a system, based upon theoretical considerations, to be in a particular regime and then gives (analytical)

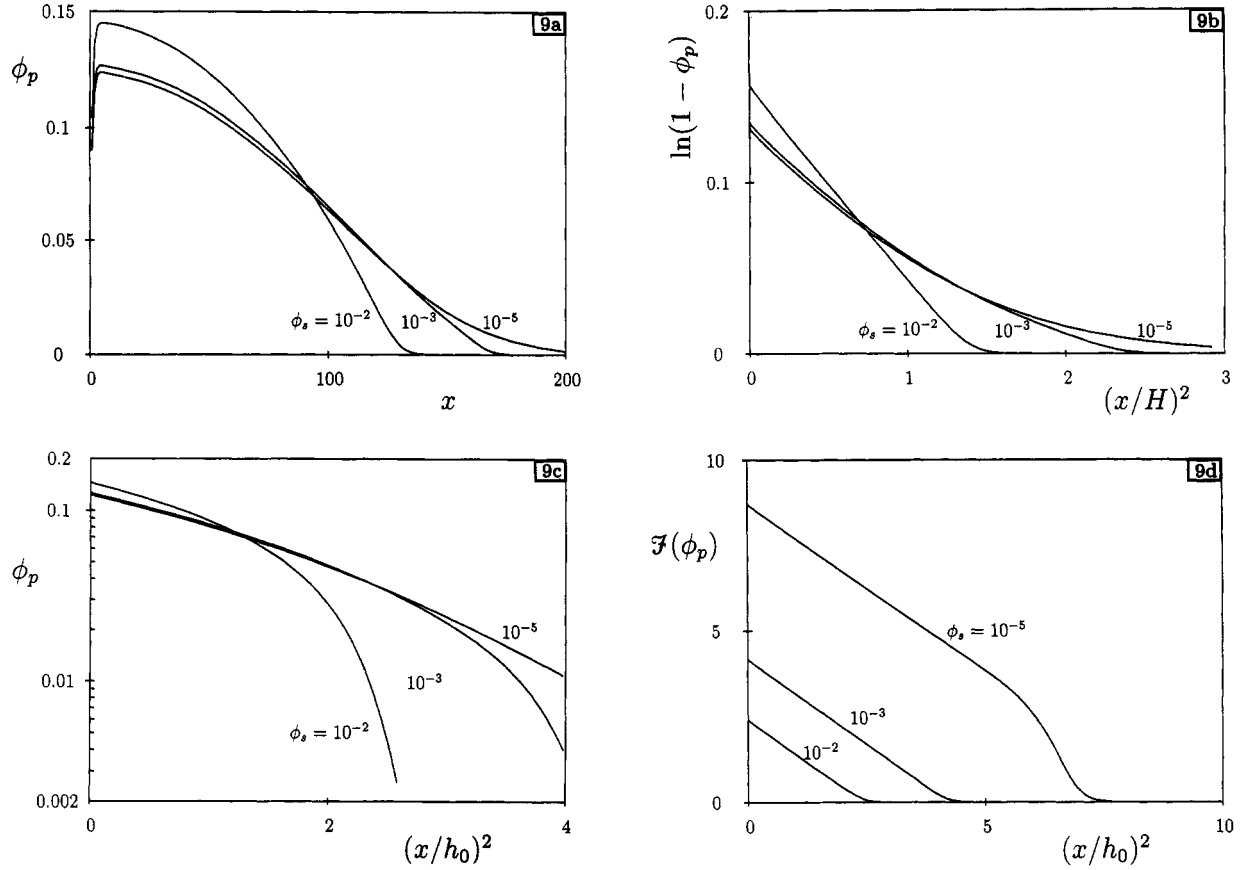

Figure 9. Volume fraction profiles ϕ_p of a charged brush at different salt concentrations ϕ_s (indicated), for $N = 500$, $\sigma = 40$, and $m = 10$. In a ϕ_p is plotted against x on a linear scale; in b $\ln(1 - \phi_p)$ is plotted against $(x/H)^2$. In such a plot a profile of a neutral brush would become a straight line. c gives $\ln \phi_p$ against $(x/h_0)^2$, so that the curves would become straight lines if only electrostatic interactions were present. Finally, d shows profiles that have been rescaled according to eq 30, i.e., $\ln \mathcal{F}(\phi_p)$ against $(x/h_0)^2$, which should lead to straight lines irrespective of the dominance of either electrostatic or nonelectrostatic interactions.

expressions for brush thickness and segment density profiles. The numerical SCF model, on the other hand, is based upon a limited set of basic assumptions (such as Poisson's law, Boltzmann's law, and the demand that the lattice be filled) but does not make presuppositions about the conformations; however, it needs to be solved numerically.

Obviously, a comparison of both methods cannot judge the validity of SCF methods in general. It does give, however, an independent proof of the validity of additional assumptions in the analytical model. On the other hand, it provides the numerical model with a framework to interpret the results of the calculations. Without such a framework, a numerical model is of limited value.

One fundamental difference between the two models is the fact that *intra*molecular and *inter*molecular interactions are distinguished explicitly in the analytical theory, whereas they are collected into one mean field in the numerical model. The latter mean-field approximation breaks down at low densities; more precisely, the OrS (oriented sticks) and IS (isotropically distributed sticks) regimes, where individual brush molecules are stretched due to intramolecular electrostatic repulsion, cannot be found from the numerical model. In addition, the NC (quasi-neutral nonoverlapping coils) regime, where chains behave as isolated uncharged coils and the size scales as $N^{3/5}$, is treated as a Gaussian regime, the size scaling with a (incorrect) mean-field exponent $^1/_2$.

Despite these minor (and expected) differences, we find excellent agreement in the three most important regimes. For the scaling of the brush thickness with either N (chain length), m (inverse charge density), σ (inverse grafting density), or ϕ_s (salt concentration), in each of the NB (quasi-neutral), OsB (osmotic brush), and SB (salted brush) regimes, complete agreement between the two theories is found. Even the exponents of the expressions giving the boundaries between the various regimes predicted by the analytical model are fully recovered in the numerical calculations.

A special remark is due on what may be called the *Pincus brush* (PB) regime.[2,4] The very peculiar scaling $H \sim N^3/\sigma m^2$ in this regime is not found from the numerical calculations. Closer investigation, using relatively short chain lengths, shows, however, that we can find a regime that is reminiscent of the PB regime. Moreover, with increasing chain length, calculated exponents change in the direction of the predicted values. To find the proper PB regime, we might have to go to very large chain lengths, but (in order to stay in the PB regime) also to lower salt concentrations, with ϕ_s scaling as $1/N^2$. Our conclusion is that, even though the theoretical considerations leading to this regime are probably correct, the numerical model will never show the typical PB behavior, since salt concentrations cannot be chosen arbitrarily low. The lower limit on salt concentrations in the numerical model is set by numerical convergence problems. Although these numerical problems have no physical relevance, a lower limit on the salt concentration does exist in real systems as well. We therefore expect that PB behavior will be very hard to find experimentally.

A second remark must be made on the transition regions. We find the transition regions to be relatively large: in major parts of the parameter space the behavior should be classified as intermediate between two limiting cases: the analytical power law behavior is recovered for relatively extreme values of charge and anchoring density only.

Consequently, we do not expect the analytical model to predict the exact value of exponents to be found experimentally, nor do we even expect experiments to reveal true power law behavior. What it can predict is a range in which exponents may be expected to fall, as well as the direction in which they will change. In short, the primary gain of the analytical theory is not the exact prediction of experimental results but the provision of a qualitative physical interpretation for them.

A convincing proof of the agreement between the two theories can be obtained by a rescaling of the segment density profiles. Although the analytical model cannot give a closed expression for the density profile in each of the regimes, it does provide a rescaling procedure, transforming each profile into a straight line when plotted in the appropriate way. If we apply this procedure to profiles calculated using the numerical model, we find indeed lines with the correct slope in the three most important regimes: NB, OsB, and SB.

From a theoretical point of view, the conclusion is that the assumptions leading to the OsB, NB, and SB expressions in the analytical model are evidently correct. More specifically, (i) the charge in a brush may be assumed to be fully compensated by counterions in the OsB and SB regimes (equivalent to the local electroneutrality assumption), and (ii) the elasticity of the chain can be described by a Gaussian expression over a wide range of parameters. As shown before,[21] the confinement of chain molecules to a lattice, as is done in the numerical model, does not seem to lead to a significantly deviating behavior.

Appendix. Parabolic Potential Profile

The potential profile of a brush has, to a good approximation, a parabolic shape. This was derived in 1975 by Semenov[19] for the case of brushes without solvent and extended to include solvent independently by Milner et al.[20] and Skvortsov et al.[22] We use the assumption of a parabolic potential profile in eq 8. In this appendix we present a straightforward derivation along the lines of a publication by Zhulina et al.[18]

Let us consider a brush of chains with chain length N and anchoring density σ. We split the free energy of a brush molecule in two parts: the stretching free energy F_{str} and concentration-dependent contributions $F_{conc} = f(\phi(x))$:

$$F = F_{str} + F_{conc} \tag{A1}$$

To keep the treatment general, this latter contribution will not be specified. Using the Gaussian expression $\int_0^{x'}(3/2)E(x,x')\,dx$ for the elastic free energy of one conformation, the total elastic free energy for the brush is given by:

$$F_{str} = \frac{3}{2}\int_0^H g(x')\,dx' \int_0^{x'} E(x,x')\,dx \tag{A2}$$

where $g(x')$ is the probability density to find the chain end at position $x = x'$. The quantity $E(x,x')$ gives the average stretching at position x of chains having their end segment at x'. Note that expression (A2) implies a simplification: all chain conformations having an end segment at $x = x'$ are replaced by one most probable conformation. This approximation is reasonably good for highly stretched chains: $x' \gg a\sqrt{N}$, where N is the total number of chain segments.

We have to minimize this free energy, taking into account the following two constraints:

$$\int_0^{x'} \frac{dx}{E(x,x')} = N \qquad \text{for all } 0 < x' < H \tag{A3}$$

and

$$\int_0^H \phi(x)\,dx = N/\sigma \tag{A4}$$

Only conformations that have their end segment at a distance $x' > x$ can contribute to the segment density $\phi(x)$ at distance x. This contribution is inversely proportional to the stretching of the conformation at x. Thus, $\phi(x)$ is given by:

$$\phi(x) = \frac{1}{\sigma}\int_x^H \frac{g(x')\,dx'}{E(x,x')} \tag{A5}$$

We use the Lagrange method of undetermined multipliers λ_1 and $\lambda_2(x')$ and define a new function that is to be minimized:

$$\mathcal{Y} = F_{str} + F_{conc} + \lambda_1\int_0^H \phi(x)\,dx + \int_0^H \lambda_2(x')\,dx' \int_0^{x'} \frac{dx}{E(x,x')} \tag{A6}$$

We obtain from eq A5:

$$\delta\phi(x) = \frac{1}{\sigma}\int_x^H dx' \left\{\frac{\delta g(x')}{E(x,x')} - \frac{g(x')\,\delta E(x,x')}{E(x,x')^2}\right\} \tag{A7}$$

which can be used to calculate the variation of $\mathcal{Y}$ with respect to the unknown functions $E(x,x')$ and $g(x')$. The terms in δE and δg are collected separately:

$$\delta\mathcal{Y} = \int_0^H \int_0^{x'} dx'\,dx\,\delta E\left\{\frac{3}{2}g(x') - \frac{\lambda_2(x')}{E(x,x')} - \left(\frac{df(x)}{d\phi(x)} + \lambda_1\right)\frac{g(x')}{E(x,x')^2}\right\} + \int_0^{x'} dx'\,\delta g\left\{\int_0^{x'}\left[\frac{3E(x,x')}{2} + \frac{1}{E(x,x')}\left(\frac{\delta f(x)}{\delta\phi(x)} + \lambda_1\right)\right]dx\right\} \tag{A8}$$

Both terms must be zero for all δE and δg, which for the δE term leads to:

$$\frac{3}{2}E^2(x,x') = \left[\frac{\delta f(x)}{\delta\phi(x)} + \lambda_1\right] + \frac{\lambda_2(x')}{g(x')} \tag{A9}$$

Realizing that the stretching $E(x,x')$ is zero at the end segment, i.e., for any $x = x'$, we can rewrite the two terms on the right-hand side of eq A9 using an unknown function $\Psi(x)$ as:

$$E^2(x,x') = \Psi(x') - \Psi(x) \tag{A10}$$

If we substitute this equation once again in the boundary condition (A3), we arrive at a standard integral equation for $\Psi(x)$, the solution of which can easily be checked to be:

$$\Psi(x) = \frac{\pi^2}{4N^2}x^2 \tag{A11}$$

Combination of this result with eq A9 leads to:

$$\Psi(x) = \left[\frac{\delta f(x)}{\delta\phi(x)} + \lambda_1\right] = \frac{\pi^2}{4N^2}x^2 \tag{A12}$$

or introducing a new constant Λ:

$$\frac{\delta f(\phi(x))}{\delta \phi(x)} = \Lambda - \frac{3}{8N^2}x^2 \qquad \text{(A13)}$$

References and Notes

(1) Halperin, A.; Tirrell, M.; Lodge, T. P. *Adv. Polym. Sci.* **1991**, *100*, 31.
(2) Pincus, P. *Macromolecules* **1991**, *24*, 2912.
(3) Zhulina, E. B.; Birshtein, T. M.; Borisov, O. V. *J. Phys. II* **1992**, *2*, 63.
(4) Borisov, O. V.; Birshtein, T. M.; Zhulina, E. B. *J. Phys. II* **1991**, *1*, 521.
(5) Borisov, O. V.; Priamitsin, V. A.; Birshtein, T. M. *Macromolecules* **1991**, *24*, 140.
(6) Zhulina, E. B.; Borisov, O. V.; Birshtein, T. M. *Polym. Prepr. (Am. Chem. Soc., Div. Polym. Chem.)* **1993**, *34* (1), 1016.
(7) Miklavic, S. J.; Marcelja, S. J. *J. Phys. Chem.* **1988**, *92*, 6718.
(8) Misra, S.; Varanasi, S.; Varanasi, P. P. *Macromolecules* **1989**, *22*, 4173.
(9) Zhulina, E. B.; Borisov, O. V.; Priamitsyn, V. A. *J. Colloid Interface Sci.* **1990**, *137*, 495.
(10) Scheutjens, J. M. H. M.; Fleer, G. J. *J. Phys. Chem.* **1979**, *83*, 1619.
(11) Scheutjens, J. M. H. M.; Fleer, G. J. *J. Phys. Chem.* **1980**, *84*, 178.
(12) Cosgrove, T.; Heath, T.; van Lent, B.; Leermakers, F. A. M.; Scheutjens, J. M. H. M. *Macromolecules* **1987**, *20*, 1692.
(13) Evers, O. A.; Fleer, G. J.; Scheutjens, J. M. H. M.; Lyklema, J. *J. Colloid Interface Sci.* **1986**, *111*, 446.
(14) Böhmer, M. R.; Evers, O. A.; Scheutjens, J. M. H. M. *Macromolecules* **1990**, *23*, 2288.
(15) Zhulina, E. B.; Israëls, R.; Fleer, G. J. *Colloids Surf.*, in press.
(16) Wittmer, J.; Joanny, J.-F. *Macromolecules* **1993**, *26*, 2691.
(17) Flory, P. J. *Principles of Polymer Chemistry*; Cornell University Press: Ithaca, NY, 1953.
(18) Zhulina, E. B.; Borisov, O. V.; Brombacher, L. *Macromolecules* **1991**, *24*, 4679.
(19) Semenov, A. N. *Sov. Phys., JETP* **1985**, *61*, 733.
(20) Milner, S. T.; Witten, T. A.; Cates, M. E. *Macromolecules* **1988**, *21*, 2610.
(21) Wijmans, C. M.; Scheutjens, J. M. H. M.; Zhulina, E. B. *Macromolecules* **1992**, *25*, 2657.
(22) Skvortsov, A. M.; Parlushvov, I. V.; Gorbunov, A. A.; Zhulina, E. B.; Pryamitsyn, V. A.; Borisov, O. V. *Polym. Sci. USSR* **1988**, *30*, 1706.